Li_2PbGeS_4 and Li_2EuGeS_4: Polar Chalcopyrites with a Severe Tetragonal Compression

Jennifer A. Aitken,[†] Paul Larson,[‡] S. D. Mahanti,[‡] and Mercouri G. Kanatzidis*[,†]

Department of Chemistry and Center for Fundamental Materials Research and Department of Physics and Astronomy and Center for Fundamental Materials Research, Michigan State University, East Lansing, Michigan 48824

Received June 1, 2001. Revised Manuscript Received September 4, 2001

Li_2PbGeS_4 and Li_2EuGeS_4 form by dissolving Pb/Eu and Ge in molten Li_2S_9 at 600−650 °C. They crystallize in the tetragonal, noncentrosymmetric space group *I-42m* with a = 6.5224(5) Å, c = 7.7603(8) Å, Z = 2, R1 = 0.0253, and wR2 = 0.0646 for Li_2PbGeS_4 and a = 6.5447(4) Å, c = 7.6960(6) Å, Z = 2, R1 = 0.0224, and wR2 = 0.0551 for Li_2EuGeS_4. These polar compounds possess a compressed chalcopyrite-like structure. The compression occurs along the c axis and results in an expanded coordination sphere for Pb and Eu that can be described as a distorted dodecahedron. The Pb/EuS_8 dodecahedra share edges and corners with the GeS_4 tetrahedra in such a way as to create small tunnels down the c axis in which the lithium cations reside. The Li^+ cations are surrounded by four S^{2-} anions that create a highly distorted tetrahedral pocket. Both compounds are semiconductors with indirect band gaps of 2.41 and 2.54 eV, respectively. We also discuss the results of an LAPW band structure calculation for Li_2PbGeS_4 and report infrared spectroscopic characterization.

Introduction

Low-melting alkali metal polychalcogenide fluxes have proven to be an outstanding tool for discovering new ternary and quaternary chalcogenides.[1,2] Despite the large number of new compounds discovered with this method, synthetic investigations have so far almost neglected the use of the lighter alkali metals. In general, it is more challenging to obtain compounds containing Li and Na because as the size of the alkali metal decreases, the basicity of the flux decreases along with the probability that the alkali metal will be incorporated in the final product.[1b] The Li−S bonds become more covalent and the nucleophilicity of the terminal S atoms of the S_x^{2-} chains decreases. In many cases, the Li ion does not get stoichiometrically incorporated into the product, making these fluxes suitable for obtaining alkali metal-free phases. For example, in the Li−Eu−Se system, only $EuSe_2$ could be obtained.[3] However, in several other cases, lithium polychalcogenide fluxes proved successful in incorporating Li^+, yielding new lithium-containing phases such as LiAuS,[4,5] Li_3AuS_2,[5] Li_4GeS_4,[6] $Li_{0.5}Pb_{1.75}GeS_4$[7], and $LiEuPSe_4$.[8]

The new compounds Li_2PbGeS_4 and Li_2EuGeS_4 represent another example in which Li incorporation is successful. They crystallize in the tetragonal noncentrosymmetric space group *I-42m* and possess a severely compressed chalcopyrite-like structure. A review of the literature showed several other compounds with similar structures, namely, KAg_2SbS_4,[9] KAg_2AsS_4,[10] $(NH_4)Ag_2AsS_4$,[11] Ag_2BaGeS_4,[12] Li_2CaGeO_4[13], and Li_2CaSiO_4.[13] These along with the two described in this paper are discussed collectively and under the same structural context for the first time as they all are *compressed* chalcopyrites. Materials with chalcopyrite-like structures are useful for a variety of applications. In the past decade, the ternary chalcopyrite 136_4[14] semiconductors have come into prominence because of their potential for nonlinear optics[15] and photovoltaic applications.[16] Here, we report the synthesis, structure, and optical properties of the semiconductors Li_2PbGeS_4 and Li_2-

* To whom correspondence should be addressed.
[†] Department of Chemistry and Center for Fundamental Materials Research.
[‡] Department of Physics and Astronomy and Center for Fundamental Materials Research.

(1) Kanatzidis, M. G. *Chem. Mater.* **1990**, *2*, 353−363. (b) Kanatzidis, M. G.; Sutorik, A. C. *Prog. Inorg. Chem.* **1995**, *43*, 151−265. (c) Kanatzidis, M. G. *Curr. Opin. Solid State Mater. Sci.* **1997**, *2* (2), 139−149.
(2) (a) Sunshine, S. A.; Kang, D.; Ibers, J. A. *J. Am. Chem. Soc.* **1987**, *109*, 6202−6204. (b) Pell, M. A.; Ibers, J. A. *Chem. Ber.* **1997**, *130*, 1−8. (c) Bensch, W.; Durichen, P. *Chem. Ber.* **1996**, *129*, 1207−1210.
(3) Aitken, J. A.; Cowen, J. A.; Kanatzidis, M. G. *Chem. Mater.* **1998**, *10*, 3928−3935.
(4) Axtell, E. A.; Liao, J.-H.; Kanatzidis, M. G. *Inorg. Chem.* **1998**, *37*, 5583−5587.
(5) Huang, F. Q.; Yang, Y.; Flaschenriem, C.; Ibers, J. A. *Inorg. Chem.* **2001**, *40*, 1397−1398.
(6) Matsushita, Y.; Kanatzidis, M. G. *Z. Naturforsch.* **1998**, *53b*, 23−30.
(7) Aitken, J. A.; Marking, G. A.; Evain, M.; Iordanidis, L.; Kanatzidis, M. G. *J. Solid State Chem.* **2000**, *153*, 158−169.
(8) Aitken, J. A.; Chondroudis, K.; Young, V. G., Jr.; Kanatzidis, M. G. *Inorg. Chem.* **2000**, *39*, 1525−1533.
(9) Schimek, G. L.; Pennington, W. T.; Wood, P. T.; Kolis, J. W. *J. Solid State Chem.* **1996**, *123*, 277−284.
(10) Schimek, G. L.; Kolis, J. W. *Acta Crystallogr.* **1997**, *C53*, 991−992.
(11) Auernhammer, M.; Effenberger, H.; Irran, E.; Pertlik, F.; Rosenstingl, J. *J. Solid State Chem.* **1993**, *106*, 421−426.
(12) Teske, C. L. *Z. Naturforsch.* **1979**, *34b*, 544−547.
(13) Gard, J. A.; West, A. R. *J. Solid State Chem.* **1973**, *7*, 422−427.
(14) In this notation, the large number represents the number of valence electrons for a particular atom and the subscripted number represents the number of such atoms in the formula.
(15) $AgGaS_2$ and $AgGeSe_2$: Catella, G. C.; Burlage, D. *MRS Bull.* **1998**, *23*, 28−36.

10.1021/cm0105357 CCC: $20.00
Published on Web 11/27/2001

$EuGeS_4$ as well as the results of electronic band structure calculation for the Pb analogue.

Experimental Section

Reagents. The chemicals in this work were used as obtained as follows unless noted otherwise: (i) lithium metal rods, 99.9%, 12.7 mm diameter, Aldrich Chemical Co., Inc., Milwaukee, WI; (ii) lead metal powder, 200 mesh, Spectrum, Gardena, CA; (iii) europium metal powder 99.9%, <250 micron, Alfa Aesar, Ward Hill, MA or europium metal chunk 99.9%, Chinese Rare Earth Information Center, Inner Mongolia, China; (iv) germanium metal powder 99.999%, 100 mesh, Alfa-Aesar, Ward Hill, MA.

Synthesis of Li_2S. Li_2S was prepared using a modified literature procedure.[17] In an argon-filled drybox, 10.085 g (0.315 mol) of sulfur was combined with 4.366 g (0.629 mol) of freshly cut lithium metal and placed in a 1000 mL round-bottom flask containing a Teflon coated stir bar. An atmosphere of argon is needed instead of nitrogen because lithium reacts readily with nitrogen to form a lithium nitride coating that renders the Li pieces insoluble. Liquid ammonia was condensed into the flask at −78 °C (dry ice and acetone bath) under argon, until the flask was two-thirds full, to give a dark blue-bronze solution. The solution was allowed to stir for 1 day, and then the ammonia was evaporated as the bath warmed to room temperature. The light yellow solid (almost 100% yield) was dried under vacuum overnight and ground to a fine powder with a mortar and pestle under a dry nitrogen atmosphere in a Vacuum Atmospheres Dri-Lab glovebox.

Preparation of Li_2PbGeS_4. In a nitrogen-filled glovebox, 0.062 g (0.3 mmol) Pb, 0.022 g (0.3 mmol) Ge, 0.014 g (0.3 mmol) Li_2S, and 0.077 g (2.4 mmol) of S were loaded into a graphite tube.[18] The graphite tube was inserted into a 13-mm-fused silica tube and flame-sealed under vacuum (approximately 2×10^{-4} mbar). This tube was heated from 50 °C to 600 °C in 24 h. The reaction was kept at this temperature for 72 h and then cooled at a rate of 2.5 °C/h to 250 °C followed by rapid cooling to 50 °C in 2 h. *N*,*N*-dimethylformamide was used to remove the excess flux, and washing with ether revealed 60% yellow polyhedra and 40% large silvery chunks. Analysis of the silver material using semiquantitative energy dispersive spectroscopy (EDS) attached to a scanning electron microscope (SEM) indicated PbS. Analysis performed on several of the yellow crystals indicated the presence of Pb, Ge, and S in an approximate 1:1:4 molar ratio. The Li content was inferred from the solution of single-crystal X-ray data and charge considerations, since Li cannot be detected by EDS. The powder diffraction pattern of the bulk sample indicated the presence of Li_2PbGeS_4 and PbS. Li_2PbGeS_4 decomposes in water immediately and within a day upon exposure to moist air.

Preparation of Li_2EuGeS_4. In a nitrogen-filled glovebox, 0.046 g (0.3 mmol) Eu, 0.022 g (0.3 mmol) Ge, 0.014 g (0.3 mmol) Li_2S, and 0.077 g (2.4 mmol) of S were loaded into a graphite tube. The graphite tube was inserted into a 13-mm silica tube and flame-sealed under vacuum (approximately 2×10^{-4} mbar). This tube was heated from 50 °C to 650 °C in 24 h. The reaction was kept at this temperature for 96 h and then cooled at a rate of 2 °C/h to 250 °C followed by rapid cooling to 50 °C in 3 h. ~60% of the product, isolated with DMF, was yellow polyhedra, while 40% was silvery dark red chunks. EDS analysis obtained from several of the yellow polyhedra gave a consistent Eu:Ge:S ratio of approximately 1:1:4. The Li content was inferred from the solution of single-crystal X-ray data and charge considerations, since Li cannot be detected by EDS. EDS analysis performed on several of the silvery dark red chunks gave an average composition of $Eu_{1.7}GeS_{4.1}$ consistent with $Li_{0.5}Eu_{1.75}GeS_4$.[19] The powder diffraction pattern of the yellow product (which could be easily separated from the silvery red chunks under light microscope) was indexed to Li_2EuGeS_4. This new phase decomposes in water and is sensitive to moist air.

Physical Measurements and Calculations. *X-ray Powder Diffraction.* Analyses were performed using a calibrated CPS 120 INEL X-ray powder diffractometer equipped with a position-sensitive detector, controlled by an IBM computer, operating at 40 kV/25 mA with a flat geometry, and employing Cu Kα radiation. Observed powder patterns were compared with powder patterns that were calculated with the Cerius2 software package.[20]

Electron Microscopy. Semiquantitative microprobe analyses of the compounds were performed with a JEOL JSM-35C Scanning Electron Microscope (SEM) equipped with a Tracor Northern Energy Dispersive Spectroscopy (EDS) detector. Data were acquired with an accelerating voltage of 20 kV and a 40 s accumulation time.

Single-Crystal UV/Vis. Optical transmission measurements were made at room temperature on single crystals using a Hitachi U-6000 microscopic FT spectrophotometer with an Olympus BH-2 metallurgical microscope over a range of 380−900 nm. Because the compounds were air-sensitive, the crystals were placed on a glass slide and covered with mineral oil for the measurement.

Infrared Spectroscopy. FT-IR spectra were recorded as solids in a CsI matrix. The samples were ground with dry CsI into a fine powder and pressed into translucent pellets. The spectra were recorded in the far-IR region (600−100 cm^{-1}, 4 cm^{-1} resolution) with the use of a Nicolet 740 FT-IR spectrometer equipped with a TGS/PE detector and silicon beam splitter.

Electronic Structure Calculations. Electronic structure calculations were performed using the self-consistent full-potential linearized augmented plane-wave method[21] (LAPW) within density functional theory[22] using the generalized gradient approximation of Perdew, Burke, and Ernzerhof[23] for the exchange and correlation potential. The calculations were performed using the WIEN97 package.[24a] The values of the atomic radii were taken to be the same for all atoms, 2.08 au, so as to fill the space between the atoms, where au is the atomic unit (0.52 Å). Adjustments of these parameters within a reasonable range showed little dependence on this variation. Convergence of the self-consistent iterations was performed for 24 k points inside the reduced Brillouin zone to within 0.0001 Ry where GMAX[25] was 10 and RKMAX[25] was 8 $bohr^{-1}$. Scalar relativistic corrections were added and spin−orbit interaction was incorporated using a second variational procedure.[26]

Single-Crystal X-ray Crystallography. *Li_2PbGeS_4 and Li_2EuGeS_4.* A platelike yellow crystal with dimensions of 0.26 × 0.14 × 0.05 mm for Li_2PbGeS_4 and a polyhedral crystal with dimensions of 0.39 × 0.36 × 0.31 mm for Li_2EuGeS_4 were

(16) $CuInSe_2$: (a) Birkmire, R. W.; Eser, E. *Annu. Rev. Mater. Sci.* **1997**, *27*, 625−653. (b) Bloss, W. H.; Pfisterer, F.; Schubert, M.; Walter, T. *Prog. Photovoltaics* **1995**, *3*, 3−24. (c) Rockett, A.; Abouelfotouh, F.; Albin, D.; Bode, M.; Ermer, J.; Klenk, R.; Peterson, T. M. *Thin Solid Films* **1994**, *237*, 1−11.

(17) Feher, F. In *Handbuch der Präparativen Anorganischen Chemie*; Brauer, G., Ed.; Ferdinand Enke: Stuttgart, Germany, 1954; vol 1, pp 280−281.

(18) The graphite tube is used to prevent reactions with the silica tube.

(19) $Li_{0.5}Eu_{1.75}GeS_4$ is X-ray isomorphous to $Li_{0.5}Pb_{1.75}GeS_4$. Iyer, R. G.; Aitken, J. A.; Kanatzidis, M. G., work in progress.

(20) *CERIUS2*, version 2.0; Molecular Simulations Inc.: Cambridge, England, 1995.

(21) Singh, D. *Planewaves, Pseudopotentials, and the LAPW Method*; Kluwer Academic: Boston, 1994.

(22) Hohenberg, P.; Kohn, W. *Phys. Rev.* **1964**, *136*, B864−B871. (b) Kohn, W.; Sham, L. *Phys. Rev.* **1965**, *140*, A1133−A1138.

(23) Perdew, J. P.; Burke, K.; Ernzerhof, M. *Phys. Rev. Lett.* **1996**, *77*, 3865−3868.

(24) Blaha, P.; Schwarz, K.; Luitz, J. *WIEN97, A Full Potential Linearized Augmented Plane Wave Package for Calculating Crystal Properties*; Karlheinz Schwarz: Techn. Universitat Wien, Austria, 1999.

(25) RKMAX is the product of the muffin tin radii (R) multiplied by the largest **k** vector in the planewave expansion (KMAX) when proper units are involved. GMAX is the largest angular momentum in the expansion of the atomic orbitals.

(26) Koelling, D. D.; Harmon, B. *J. Phys.* **1980**, *C13*, 6147.

Table 1. Crystallographic Data for Li_2PbGeS_4 and Li_2EuGeS_4

formula	Li_2PbGeS_4	Li_2EuGeS_4
formula weight	421.90	366.67
crystal habit, color	platelike, yellow	polyhedra, yellow
space group	I-42m	I-42m
a, Å	6.5224(5)	6.5447(4)
c, Å	7.7603(8)	7.6960(6)
Z; V, Å^3	2,330.14(5)	2,329.64(4)
D (calc), g/cm^3	4.244	3.694
temp, K	173	173
λ, Å	0.71073 (Mo Kα)	0.71073 (Mo Kα)
μ, mm^{-1}	31.146	15.115
F(000)	368	330
θ_{max}, deg	26.97	28.26
total data measd.	1626	1060
total unique data	203 R(int) = 0.083	226 R(int) = 0.047
parameters	14	14
refinement method	full-matrix least-squares on F^2	
extinction coeff.	0.072(6)	0.35(2)
R indices (all data)	R1[a] = 0.0253, wR2[b] = 0.0646	R1[a] = 0.0224, wR2[b] = 0.055
goodness of fit on F^2	1.11	1.14

[a] $R1 = \sum||F_o| - |F_c||/\sum|F_o|$. [b] $wR2 = \{\sum[w(F_o^2 - F_c^2)^2]/\sum[w(F_o^2)^2]\}^{1/2}$.

mounted on glass fibers. A Bruker SMART Platform CCD diffractometer, operating at 50 kV/40 mA and using graphite monochromatized Mo Kα radiation at 173 K, was used for data collection. A full sphere of data was collected with 0.30° steps in ω and an exposure time of 30 s/frame for the Pb compound and 20 s/frame for the Eu compound. No crystal decay was detected. The SMART[27] software was used for data acquisition and the SAINT[27] program was used for data extraction. The final cell constants were determined from a set of 4391 (Li_2PbGeS_4) or 1267 (Li_2EuGeS_4) strong reflections [$I > 10\sigma(I)$] obtained from data collection. Both crystals were very strongly diffracting, and all measured reflections were greater than $2\sigma(I)$.

An empirical absorption correction was done using SADABS,[28] and all refinements were done using the SHELXTL[29] package of crystallographic programs. The systematic absences pointed to eight possible space groups. The three choices with the lowest CFOM (combined figure of merit) were *I-4* (acentric), *I-42m* (acentric), and *I*4/*mmm* (centric). The intensity statistics indicated a noncentrosymmetric space group; therefore, we proceeded with *I-42m* first since it belongs to the higher symmetry Laue class (*4*/*mmm*). All atoms were revealed within three rounds of least-squares/difference Fourier cycles. In the initial stages of refinement, the incorrect enantiomorphs were selected; therefore, the coordinates were inverted and the refinement proceeded. All atoms were located (R1 = 0.0558 and wR2 = 0.1409 for Li_2PbGeS_4 and R1 = 0.0898 and wR2 = 0.2454 for Li_2EuGeS_4) and subsequently refined anisotropically (R1 = 0.0511 and wR2 = 0.1409 for Li_2PbGeS_4 and R1 = 0.0867 and wR2 = 0.2399 for Li_2EuGeS_4). After introducing an extinction coefficient, the R values dropped dramatically to R1 = 0.0253 and wR2 = 0.645 for Li_2PbGeS_4 and R1 = 0.0224 and wR2 = 0.0551 for Li_2EuGeS_4. The maximum and minimum peaks on the final Fourier difference map corresponded to 1.536 and −1.482 e$^-$/Å^3 for Li_2PbGeS_4 and 1.901 and −0.679 e$^-$/Å^3 for Li_2EuGeS_4, respectively. Crystallographic data for Li_2PbGeS_4 and Li_2EuGeS_4 are given in Table 1, and fractional atomic coordinates and isotropic displacement parameters are given in Table 2. A crystallographic data file in cif format is deposited as Supporting Information.

(27) *SMART and SAINT*: *Data Collection and Processing Software for the SMART system*; Siemens Analytical X-ray Instruments Inc., 1995.

(28) Sheldrick, G. M. University of Göttingen, Germany, to be published.

(29) *SHELXTL V-5*; Siemens Analytical X-ray Systems Inc.: Madison, WI.

Table 2. Atomic Coordinates and Equivalent Isotropic Displacement Parameters (Å^2 × 10^3) for Li_2PbGeS_4 and Li_2EuGeS_4

atom	Wycoff letter & multiplicity	x	y	z	*U*(eq)[a]
		Li_2PbGeS_4			
Li	4d	0	0.5	0.25	28(8)
Pb	2a	0	0	0	15(1)
Ge	2b	0	0	0.5	5(1)
S	8i	0.3030(3)	0.3030(3)	0.1624(3)	9(1)
		Li_2EuGeS_4			
Li	4d	0	0.5	0.25	14(5)
Eu	2a	0	0	0	9(1)
Ge	2b	0	0	0.5	7(1)
S	8i	0.3036(2)	0.3036(2)	0.1636(2)	10(1)

[a] *U*(eq) is defined as one-third of the trace of the orthogonalized *Uij* tensor.

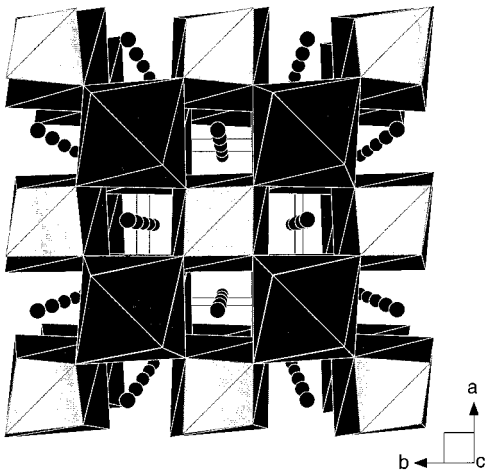

Figure 1. Polyhedral representation of the structure of Li_2PbGeS_4 viewed down the *c* axis. The PbS_8 distorted dodecahedra are shown in black, the GeS_4 tetrahedra are shown in gray, and the Li^+ cations are represented by small black circles.

Results and Discussion

Structure. The tetragonal structure adopted by both compounds is related to the chalcopyrite structure-type in an interesting fashion. First, we will describe in detail the structure of Li_2PbGeS_4, and then we will compare and contrast the europium analogue.

The structure of Li_2PbGeS_4 is a three-dimensional network of densely packed atoms, see Figure 1. The Pb atoms are bonded to eight S atoms with four short Pb−S bonds of 3.066(3) Å and four longer ones of 3.1889(3) Å, see Figure 2a. The coordination polyhedra of the Pb atoms can best be described as distorted dodecahedra that are composed of two interpenetrating distorted tetrahedra. One tetrahedron is composed of the four proximal S atoms while the four distal S atoms define the other. The PbS_8 dodecahedra alone form a three-dimensional network by corner sharing, see Figure 3a. Each PbS_8 shares eight corners with eight other PbS_8 dodecahedra. The Ge atoms reside in a near perfect tetrahedral site with Ge−S bond distances of 2.211(3) Å and an average S−Ge−S bond angle of 109.47°, see Figure 2b. The GeS_4 tetrahedra share edges with two PbS_8 polyhedra and corner share with four other PbS_8 polyhedra to create small tunnels down the *c* axis in which the Li^+ cations reside, see Figure 1. The lithium atoms are surrounded by four S atoms at a distance of

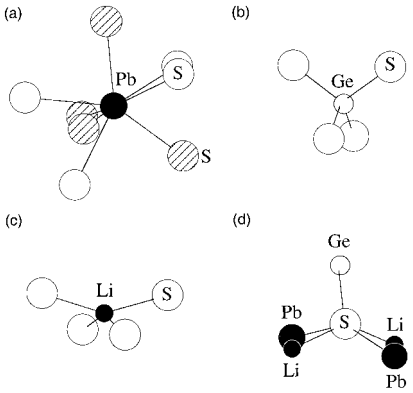

Figure 2. The immediate coordination spheres of (a) Pb, (b) Ge, (c) Li, and (d) S in the compound Li_2PbGeS_4. In (a), the atoms with stripes represent the four proximal S atoms, and the open circles represent the four distal S atoms.

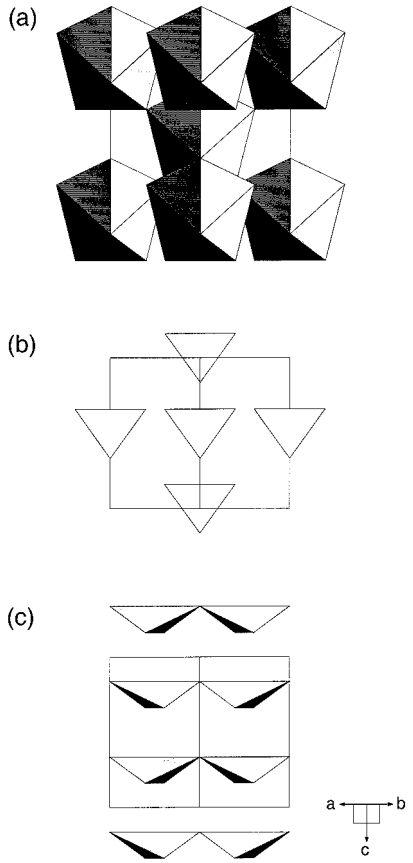

Figure 3. Polyhedral representations of (a) the corner-sharing PbS_8 distorted dodecahedra which form an infinite three-dimensional framework, (b) the arrangement of the GeS_4 tetrahedra, and (c) the spacial arrangement of the highly distorted LiS_4 tetrahedra, viewed down the [110] direction. The polar nature of the structure is apparent from the identical orientation of all polyhedra.

2.4534(9) Å, see Figure 2c. These S atoms create a highly distorted tetrahedral pocket with four S−Li−S angles of 94.40(3)° and two of 147.8(1)°. Each sulfur atom is surrounded by two Pb atoms, two Li atoms, and one Ge atom which create a highly distorted five-coordinate site that can be best described as a distorted square pyramidal pocket, see Figure 2d. The two Pb and two Li atoms create the square base with two Pb−S−Pb bond angles of 86.11(6)° and two Pb−S−Li angles of 83.447(6)°. The Ge atom serves as the top of the pyramid. It is easy to see, when looking down the [110] direction, that none of the polyhedra in the structure are related by a center of symmetry and that the PbS_8 dodecahedra, GeS_4 tetrahedra, and LiS_4 tetrahedra all point in the same direction, see Figure 3.

The structure of Li_2EuGeS_4 is nearly identical to that of Li_2PbGeS_4 since the distances and angles differ only slightly, see Table 3. The "largest" difference between the two compounds is in the Pb/Eu−S distances. In Li_2EuGeS_4, the Eu coordination sphere is more symmetrical (4 × 3.080(2) Å and 4 × 3.163(2) Å) than that observed for Pb in Li_2PbGeS_4.

Relationship to Chalcopyrite. The structure of Li_2PbGeS_4 and Li_2EuGeS_4 can be derived from the diamond-like ZnS structure (sphalerite-type ZnS, also called zinc blende). The chalcopyrite structure-type ($CuFeS_2$[30]) with the space group symmetry *I-42d* is an ordered superstructure of ZnS with the Zn atoms being replaced alternately with Cu and Fe atoms in a regular fashion, see Figure 4a and b. Another possibility when distributing two cations over the Zn site is for one type of cation to be stabilized in two different crystallographic sites while the other cation finds only one site. An example of this is the mineral famatinite, Cu_3SbS_4.[31] In this case, two-thirds of the Cu atoms sit on one crystallographic site, while one-third is on another site; the Sb resides on a third site dropping the space group symmetry to *I-42m*. If three cations are distributed over the Zn site of sphalerite in an ordered way such that the average valence electrons per anion is still 8, the space group symmetry will also result in *I-42m*. For example, this type of structure is observed in the mineral stannite, Cu_2FeSnS_4.[32] The types of structural relationships shown here exist for a myriad of compounds and have been discussed previously in the literature.[33]

When going from sphalerite to chalcopyrite, a small distortion along the *c* axis, known as a tetragonal compression, is observed. This is due to the difference in the radii of the two cations which distorts the lattice such that the unit cell height becomes slightly less than twice the base dimension. The quantity 2-(*c*/*a*) is a measure of the tetragonal distortion. Table 4 lists the *c*/*a* ratios for a number of compounds. The 2-(*c*/*a*) values for chalcopyrite ($CuFeS_2$), $AgGaS_2$,[34] $AgGaSe_2$[34], and $CuInSe_2$[35] are small or zero. The 2-(*c*/*a*) values for famatinite (Cu_3SbS_4) and stannite (Cu_2FeSnS_4) are also small or zero since the cationic radii in these two compounds are relatively similar; thus, they can be considered as more or less ideal derivatives of the

(30) Kratz, T.; Fuess, H. *Z. Kristallogr.* **1989**, *186*, 167−169.
(31) Garin, J.; Parthe, E.; Oswald, R. *Acta Crystallogr.* **1972**, *B28*, 3672−3674.
(32) Hall, S. R.; Szymanski, J. T.; Stewart, J. M. *Can. Mineral.* **1978**, *16*, 131−137.
(33) (a) Goryunova, N. A. In *The Chemistry of Diamond-Like Semiconductors*; Anderson, J. C., Ed.; MIT Press: Massachusetts, 1965. (b) Parthé, E.; Yvon, K.; Deitch, R. H. *Acta Crystallogr.* **1969**, *B25*, 1164. (c) Parthé, E. *Elements of Inorganic Structural Chemistry*; K. Sutter Parthe: Lancy, Switzerland, 1996; pp 41−58 and references therein. (d) Parthé, E. In *Intermetallic Compounds: Vol. 1, Principles*; Westbrook, J. H., Fleischer, R. L., Eds.; John Wiley and Sons Ltd: New York, 1994; pp 343−360 and references therein. (e) Wold, A.; Dwight, K. Chalcogenides with the Tetrahedral Structure. *Solid State Chemistry*; Chapman and Hall: New York, 1993. (f) Hauck, J.; Mika, K. *J. Solid State Chem.* **1998**, *138*, 334−341.
(34) Hahn, H.; Frank, G.; Klinger, W.; Meyer, A. D.; Stoerger, G. *Z. Anorg. Allg. Chem.* **1953**, *271*, 153−170.
(35) Zahn, G.; Paufler, P. *Cryst. Res. Technol.* **1988**, *23* (4), 499−506.

Table 3. Selected Intramolecular Distances (Å) and Angles (deg) for Li_2PbGeS_4 and Li_2EuGeS_4

	distances			angles	
	Li_2PbGeS_4	Li_2EuGeS_4		Li_2PbGeS_4	Li_2EuGeS_4
Li−S	2.4534(9) × 4	2.4581(4) × 4	S−Li−S	94.40(3) × 4	94.19(2) × 4
			S−Li−S	147.8(1) × 2	148.62(8) × 2
Pb/Eu−S	3.066(3) × 4	3.080(2) × 4	S−Pb/Eu−S	70.15(6) × 2	69.48(9) × 2
	3.188(3) × 4	3.163(2) × 4	S−Pb/Eu−S	70.26(3) × 8	70.45(2) × 8
			S−Pb/Eu−S	79.53(3) × 4	79.06(1) × 4
			S−Pb/Eu−S	99.73(4) × 4	99.63(3) × 4
			S−Pb/Eu−S	131.46(9) × 2	131.72(6) × 2
			S−Pb/Eu−S	132.48(6) × 4	132.05(4) × 4
			S−Pb/Eu−S	149.01(9) × 4	149.21(6) × 4
Ge−S	2.211(3)	2.211(2)	S−Ge−S	108.96(7) × 4	108.93(4) × 4
			S−Ge−S	110.5(1) × 2	110.57(9) × 2
			Li−S−Pb/Eu	83.45(6) × 2	83.96(4) × 2
			Li−S−Pb/Eu	86.11(6) × 2	85.78(4) × 2
			Ge−S−Pb/Eu	90.01(8)	89.64(5)
			Ge−S−Li	108.77(6) × 2	108.66(4) × 2
			Ge−S−Pb/Eu	120.0(1)	121.15(7)
			Li−S−Li	140.1(1)	140.56(7)
			Pb/Eu−S−Pb/Eu	149.01(9)	149.21(6)

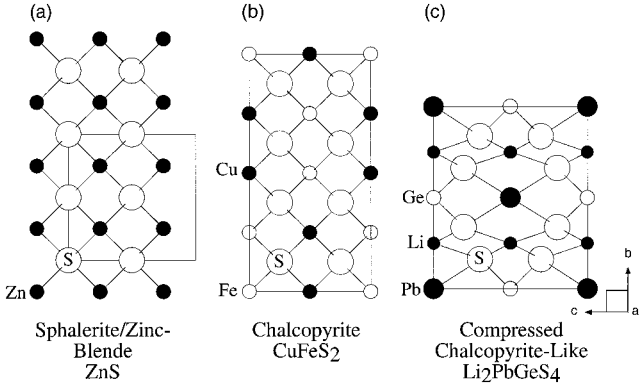

Figure 4. Structural evolution from (a) sphalerite (zinc blende-type ZnS, *F-43m*) to (b) normal chalcopyrite ($CuFeS_2$, *I-42d*) to (c) the compressed chalcopyrite-like structure of Li_2PbGeS_4 (*I-42m*).

Table 4. Selected Compounds with Normal Chalcopyrite and Compressed Chalcopyrite Structures

compound	space group	*a* (Å)	*c* (Å)	*a*/*c*	2-*a*/*c*	reference #
$CuFeS_2$	I-42d	5.2864(8)	10.4102(8)	1.97	0.003	30
$AgGaS_2$	I-42d	5.743(5)	10.26(1)	1.79	0.21	34
$AgGaSe_2$	I-42d	5.973(5)	10.88(1)	1.82	0.18	34
$CuInSe_2$	I-42d	5.781(1)	11.609(3)	2.00	0	35
Cu_3SbS_4	I-42m	5.385(1)	10.754(2)	2.00	0	31
Cu_2FeSnS_4	I-42m	5.449(2)	10.757(3)	1.97	0.003	32
Li_2PbGeS_4	I-42m	6.5224(5)	7.7603(8)	1.16	0.84	this paper
Li_2EuGeS_4	I-42m	6.5447(4)	7.6960(6)	1.18	0.82	this paper
KAg_2SbS_4	I-42m	6.886(1)	8.438(2)	1.22	0.78	9
KAg_2AsS_4	I-42m	6.7504(5)	8.265(1)	1.22	0.78	10
$(NH_4)Ag_2AsS_4$	I-42m	6.780(1)	8.277(1)	1.22	0.78	11
Ag_2BaGeS_4	I-42m	6.82(8)	8.01(7)	1.17	0.83	12
Li_2CaGeO_4	I-42m	5.141(2)	6.595(2)	1.28	0.72	13
Li_2CaSiO_4	I-42m	5.047(5)	6.486(6)	1.29	0.71	13

chalcopyrite structure-type. Larger 2-(*c*/*a*) values can be found if a severe compression along the *c* axis occurs.

The structure of stannite is also the type of structure observed for Li_2PbGeS_4 (see Figure 4c) and Li_2EuGeS_4, albeit severely compressed along the *c* axis. The *c* axis compression expands the coordination sphere of one of the cations from 4 to 8. This is the reason these phases with nontetrahedral cations are able to adopt this structure type. Therefore, Li_2PbGeS_4 and Li_2EuGeS_4 represent a severe compression with 2-(*c*/*a*) values of 0.82 and 0.84, respectively. This high degree of distortion takes place for two important reasons. The most obvious is that the cationic radii in these two compounds are very different. Furthermore, the larger Pb and Eu cations prefer a coordination number of eight rather than only four as found in ZnS, chalcopyrite, and all its ideal derivatives. In order for the larger cations to achieve their higher coordination spheres, the structure must compress itself considerably, exerting a kind of "chemical pressure" in these systems. This type of structure has also been observed for other phases such as KAg_2SbS_4,[9] KAg_2AsS_4,[10] $NH_4Ag_2AsS_4$,[11] Ag_2BaGeS_4,[12] Li_2CaGeO_4,[13] and Li_2CaSiO_4.[13]

In all of these compressed chalcopyrite compounds, the types of cations and the coordination geometries which they adopt are similar. In each compound, there exists a rather large cation whose coordination number is eight instead of only four, a medium- to small-size cation that adopts an almost perfect tetrahedral geometry, and another small cation that tolerates a highly distorted tetrahedral site. More specifically, Pb, Eu, K, NH_4, Ba, and Ca occupy the large cation site, and Sb, As, Ge, or Si cations occupy the regular tetrahedral site, while the highly distorted tetrahedral site is occupied by Li or Ag cations.

Ag_2BaSnS_4[36] and the recently reported compound $Ag_2BaGeSe_4$[37] also exhibit a compressed chalcopyrite-like structure; however, the compression results in a distortion such that the lattice symmetry is no longer tetragonal but rather orthorhombic (space group *I222*, $a = 7.127(3)$ Å, $b = 8.117(3)$ Å, and $c = 6.854(3)$ Å for Ag_2BaSnS_4 and $a = 7.058(2)$ Å, $b = 7.263(2)$ Å, and $c = 8.253(2)$ Å for $Ag_2BaGeSe_4$). Interestingly, although copper can tolerate a highly distorted tetrahedral coordination, currently there appears to be no example of a copper-containing compressed chalcopyrite. The compounds Cu_2SrSnS_4,[38] Cu_2BaGeS_4,[39] Cu_2SrGeS_4,[39] $Cu_2BaGeSe_4$,[37] and $Cu_2SrGeSe_4$[37] also possess the three types of cations required to achieve a compressed chalcopyrite structure, yet for some reason, they adopt very different structures. This is despite the fact that the local geometry of the three cations is similar to the compounds reported here (i.e., one cation is eight-

(36) Teske, C. L.; Vetter, O. *Z. Anorg. Allg. Chem.* **1976**, *427*, 200−204.
(37) Tampier, M.; Johrendt, D. *Z. Anorg. Allg. Chem.* **2001**, *627*, 312−320.
(38) Teske, C. L. *Z. Anorg. Allg. Chem.* **1976**, *419*, 67−76.
(39) Teske, C. L. *Z. Naturforsch.* **1979**, *34b*, 386−389.

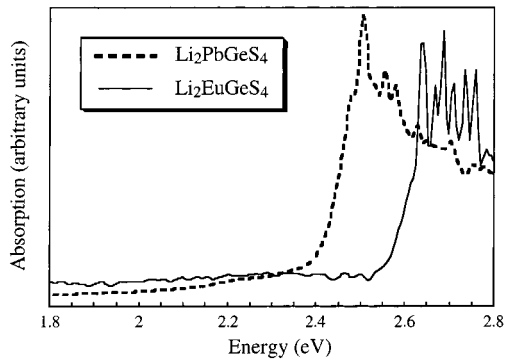

Figure 5. Single-crystal optical absorption spectra of Li_2PbGeS_4 and Li_2EuGeS_4. The sharp features at high absorbance are noise and are due to the very low transmission of light at those energies.

coordinate, one resides in regular tetrahedra, and one sits in very distorted tetrahedra).

Spectroscopy. The transparent, well-formed crystals of Li_2PbGeS_4 and Li_2EuGeS_4 were suitable for single-crystal optical transmission measurements. Both compounds exhibit sharp optical absorptions of 2.41 and 2.54 eV, respectively, see Figure 5. These energy gaps are consistent with the yellow color of these materials. Analysis of the shape of the absorption edge in these spectra can be used to distinguish between a direct and an indirect gap semiconductor.[40] In semiconductors, the energy dependence of the absorption coefficient is quadratic in materials with a direct energy gap, whereas in those with indirect gaps, the dependence scales to the square root.[41] Data plots of absorption^2 versus energy and absorption$^{(1/2)}$ versus energy using the data points at the absorption edge region are plotted in Figure 6. The absorption$^{(1/2)}$ versus energy plot is nearly linear for both Li_2PbGeS_4 and Li_2EuGeS_4, while the plot of absorption^2 versus energy deviates significantly from linearity suggesting that both compounds are *indirect* band gap semiconductors. The indirect nature of the optical band gaps in these materials is supported by electronic band structure calculations preformed for Li_2PbGeS_4 (see below).

The far-infrared spectra of both compounds are shown in Figure 7. The spectra display two strong absorptions in the region of ~400 cm^{-1} which correspond to the stretching vibrations of the $[GeS_4]^{4-}$ tetrahedron. These absorptions occur at 399 and 370 cm^{-1} for Li_2PbGeS_4 and at 408 and 377 cm^{-1} for Li_2EuGeS_4. The absorptions at lower energies, 232, 221, and 186 cm^{-1} for Li_2PbGeS_4 and 236, 194, and 160 cm^{-1} for Li_2EuGeS_4, should correspond to Pb−S or Eu−S modes, respectively. The spectral response of these materials is similar to that of $Li_{0.5}Pb_{1.75}GeS_4$[7] which also exhibits two strong absorptions at 394 and 361 cm^{-1} corresponding to the $[GeS_4]^{4-}$ tetrahedra.

Band Structure Calculations. We performed band structure calculations for Li_2PbGeS_4 at the density functional theory (DFT) level. Our aim was to obtain additional insight into the type of band gap present, the nature of the conduction and valence bands, and the origin of the yellow color observed for these materials. The fine details of the band structure are sensitive to whether spin−orbit coupling is included in the calculation. The band structure before the inclusion of spin−orbit is shown in Figure 8a. Here, the minimum in the conduction band is at the V point of the Brillouin zone and the maximum in the valence band is at point M

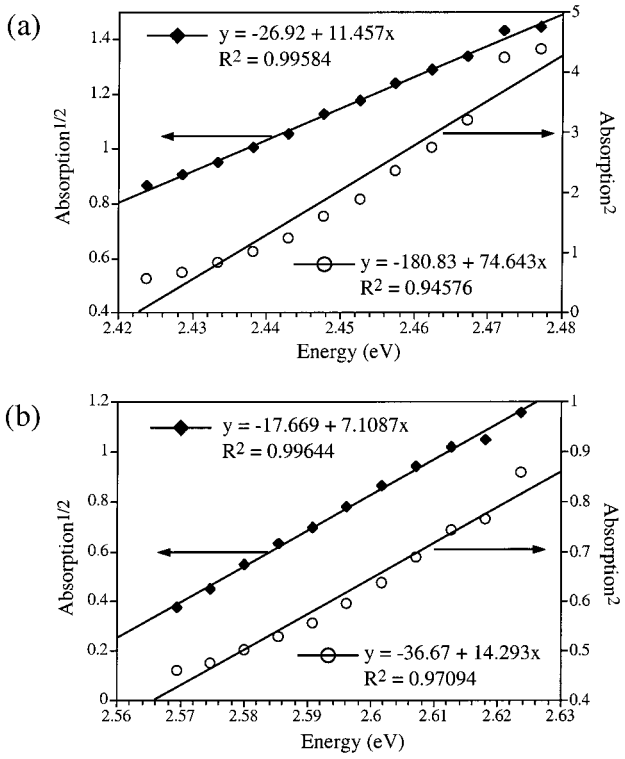

Figure 6. (a) The absorption edge data of Li_2PbGeS_4 plotted as absorption^2 vs energy (direct gap) and absorption$^{1/2}$ vs energy (indirect gap). (b) Corresponding plots for Li_2EuGeS_4. The band gap is obtained by extrapolation of the linear region of the absorption edge (indirect gap model) to zero absorption.

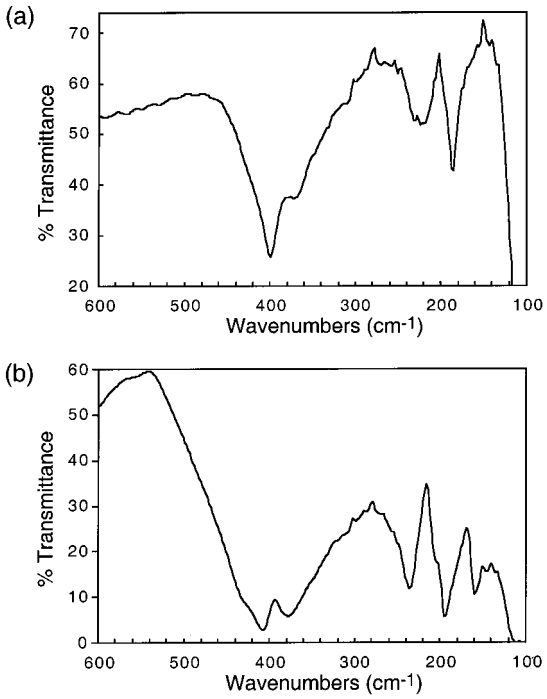

Figure 7. Far-infrared spectra of (a) Li_2PbGeS_4 and (b) Li_2EuGeS_4.

(40) This type of analysis is only valid if single-crystal spectra are available. It is less reliable when using diffuse reflectance data.

(41) Pankove, J. I. *Optical Processes in Semiconductors*; Dover Publications: New York, 1971; pp 34−42.

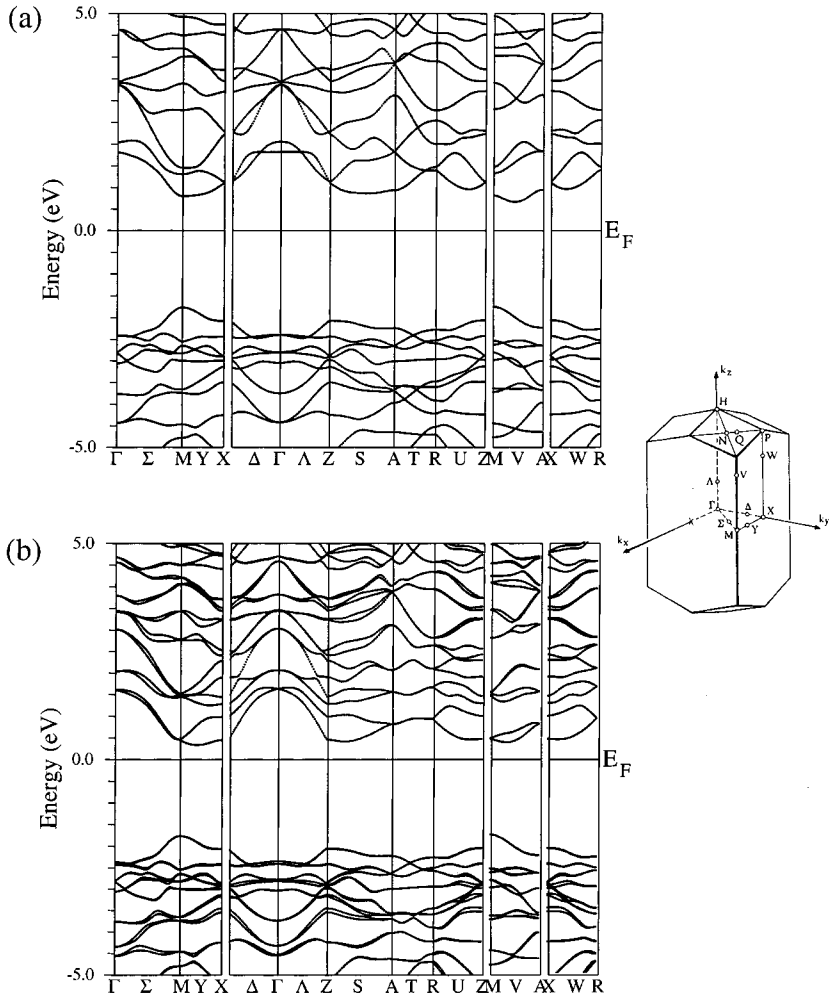

Figure 8. A portion of the electronic band structure calculated for Li_2PbGeS_4 in selected directions of reciprocal space. (a) The band structure without spin−orbit coupling. (b) The band structure with the inclusion of spin−orbit coupling. The Fermi level energy is denoted E_F. Shown on the right is the Brillouin zone and associated reciprocal space directions for the body-centered tetragonal system, adapted from Lax, M. *Symmetry Principles in Solid State and Molecular Physics*; John Wiley & Sons: New York, 1974; pp 449.

resulting in an indirect energy gap, ∼2.4 eV. A slightly higher conduction band minimum occurs along ZA near S. The inclusion of spin−orbit causes splitting of the bands, especially those of Pb character dominant in the conduction band, see Figure 8b. The conduction band minimum shifts away from the V point to a general point between M and X, producing a smaller, indirect gap of 2.09 eV. Since LAPW calculations generally underestimate energy gaps, this value is considered to be close to the experimentally determined value of 2.41 eV. More importantly, these calculations confirm the indirect nature of the band gap as suggested from the optical absorption data.

An orbital analysis of the bands shows that the Pb p, Ge p, and S p orbitals hybridize strongly near the Fermi energy. The Pb p and Ge p orbitals are found to lie mostly in the conduction band. Whereas the S p orbitals lie mostly in the valence band, there is a strong hybridization with the Pb p and Ge p orbitals. The Li s orbitals lie 4 eV above the Fermi energy; thus, the Li electrons are considered to be donated to the Pb−Ge−S framework. The hybridization of Li s with the S p orbitals is weak below the valence band maximum; therefore, the bonding of Li with the S atoms may be still considered nearly ionic. The region near the bottom of the conduction band and the top of the valence band has mostly S and Pb orbital character, respectively. On this basis, we can conclude that the lowest energy indirect band gap excitation arises from a primarily S→Pb charge-transfer transition at ∼2.4 eV resulting in the yellow color observed for these materials.

Concluding Remarks

The indirect gap semiconductors Li_2PbGeS_4 and Li_2EuGeS_4 were prepared from a lithium polysulfide flux at moderate temperatures. The successful incorporation of Li^+ in these compounds proves that fluxes of the lighter alkali metals are suitable of forming alkali-containing chalcogenides given the proper conditions. Apparently, the presence of highly Lewis acidic centers such as Ge^{4+} favors the incorporation of Li^+. The severely compressed chalcopyrite structure of Li_2PbGeS_4 and Li_2EuGeS_4 allows compositions with large metal ions of high coordination preference to be accommodated in the lattice. The flexibility of this structure type could be useful in tailoring the properties of these semiconducting materials. Since we know the types of cations that reside in each of the three different sites of this structure, it is conceivable to predict other possible

quaternary lithium (or silver) sulfides and selenides that might adopt the same structure type.

Acknowledgment. Financial support from the National Science Foundation is gratefully acknowledged. This work made use of the SEM facilities of the Center for Advanced Microscopy at Michigan State University. The Bruker SMART platform CCD diffractometer at Michigan State University was purchased with funds from the National Science Foundation (CHE-9634638). Sincere thanks to Professor Erwin Parthé for the many fruitful discussions of diamond-like structures.

Supporting Information Available: An X-ray crystallographic file, in CIF format containing information for Li_2PbGeS_4 and Li_2EuGeS_4 (SIE). This material is available free of charge via the Internet at http://pubs.acs.org.

CM0105357